FULL-LENGTH PAPER

# Impact of the PEG length and PEGylation site on the structural, thermodynamic, thermal, and proteolytic stability of mono-PEGylated alpha-1 antitrypsin

Xiao Liu[1]  |  Kobenan G. W. Kouassi[1]  |  Rita Vanbever[1] (ORCID)  |  Mireille Dumoulin[2]

[1]Advanced Drug Delivery and Biomaterials, Louvain Drug Research Institute, Université catholique de Louvain (UCLouvain), Brussels, Belgium

[2]Department of Life Sciences, InBios, Center for Protein Engineering, Nanobodies to Explore Protein Structure and Functions, University of Liège, Liège, Belgium

**Correspondence**
Rita Vanbever, Advanced Drug Delivery & Biomaterials, Louvain Drug Research Institute, Université catholique de Louvain (UCLouvain), Avenue E. Mounier, 73 boite B1.73.12, 1200 Brussels, Belgium
Email: rita.vanbever@uclouvain.be and

Mireille Dumoulin, Department of Life Sciences, InBios, Center for Protein Engineering, Nanobodies to explore Protein Structure and Fonctions, Liége, Belgium.
Email: mdumoulin@uliege.be

**Funding information**
Alpha1 Foundation, Grant/Award Number: 553700; China Scholarship Council, Grant/Award Number: 201707040053

**Review Editor:** Aitziber Cortajarena

## Abstract

Conjugation to polyethylene glycol (PEG) is a widely used approach to improve the therapeutic value of proteins essentially by prolonging their body residence time. PEGylation may however induce changes in the structure and/or the stability of proteins and thus on their function(s). The effects of PEGylation on the thermodynamic stability can either be positive (stabilization), negative (destabilization), or neutral (no effect). Moreover, various factors such as the PEG length and PEGylation site can influence the consequences of PEGylation on the structure and stability of proteins. In this study, the effects of PEGylation on the structure, stability, and polymerization of alpha1-antitrypsin (AAT) were investigated, using PEGs with different lengths, different structures (linear or 2-armed) and different linking chemistries (via amine or thiol) at two distinct positions of the sequence. The results show that whatever the size, position, and structure of PEG chains, PEGylation (a) does not induce significant changes in AAT structure (either at the secondary or tertiary level); (b) does not alter the stability of the native protein upon both chemical- and heat-induced denaturation; and (c) does not prevent AAT to fully refold and recover its activity following chemical denaturation. However, the propensity of AAT to aggregate upon heat treatment was significantly decreased by PEGylation, although PEGylation did not prevent the irreversible inactivation of the enzyme. Moreover, conjugation to PEG, especially 2-armed 40 kDa PEG, greatly improved the proteolytic resistance of AAT. PEGylation of AAT could be a promising strategy to prolong its half-life after infusion in AAT-deficient patients and thereby decrease the frequency of infusions.

**KEYWORDS**
alpha-1 antitrypsin (AAT), heat-induced aggregation, PEGylation, proteolysis, thermodynamic stability

## 1 | INTRODUCTION

Alpha-1 antitrypsin (AAT) is a serine protease inhibitor, which is predominantly expressed by hepatocytes and

then diffuses into the circulation.[1] Its primary site of action is the lung, where it provides a protection against serine proteases such as neutrophil elastase (NE),[2] proteinase-3 (PR-3),[3] and cathepsin G (Cat-G).[4] Deficiency in AAT, resulting from mutations in the *SER-PINA1* gene, can cause various diseases including hepatic disease, emphysema and chronic obstructive pulmonary disease (COPD).[1] The main approach to treat the pulmonary disease associated with AAT deficiency is the weekly intravenous infusion of human plasma-purified AAT. However, a high dose (60 mg/kg/week) is mandatory to maintain efficacious serum levels of AAT (>11 μM), which results in high expenses.[5] Moreover, in a Phase II/III clinical trial involving patients with AAT deficiency and severe COPD with frequent exacerbations, a twice-daily inhalation of 80 mg of AAT for 50 weeks did not prolong the time to exacerbation, but it significantly reduced symptomatic Anthonisen Type I exacerbations.[6] Our hypothesis to explain this limited efficacy of inhaled AAT is its rapid clearance caused by a combination of proteolytic breakdown, oxidation of methionine358 belonging to the reactive center loop (RCL) and phagocyte uptake.[6] Hence, it is necessary to develop AAT derivatives presenting longer residence time following both intravenous and pulmonary administration, as it could improve the efficacy of therapy, reduce the administration frequency, and increase the patience compliance.

Polyethylene glycol (PEG) is one of the most popular polymers for protein conjugation.[7] Several PEGylated proteins have been approved by the FDA and EMA in the pharmaceutical market.[8,9] The conjugation of PEG chains to proteins can prolong their serum half-life by decreasing the kidney clearance. It can also reduce the immunogenic response to proteins and protect them from proteolysis.[10] Despite the advantages of PEGylation for therapeutic proteins, one concern is the reduction in their biological activity and/or stability upon PEGylation. Although, in some cases, the reduced activity could be compensated by the prolonged serum half-life,[11,12] it is nevertheless of great interest for researchers to maintain the full activity of the therapeutic protein after PEGylation.[9]

Various factors such as the PEG length and the PEGylation site can influence the stability and biological activity of a PEGylated protein through conformational changes at the level of tertiary and secondary structures and/or steric hindrance of the conjugated PEG.[13] Thermodynamically-destabilized proteins tend to more easily transition to unfolded states which are generally devoid of activity and prone to aggregation.[14] Therefore, a preserved or improved thermodynamic stability is desired after PEGylation. So far, the impact of PEGylation on the thermodynamic stability of a protein has not yet been thoroughly investigated. PEGylation can stabilize, destabilize a protein, or have no effect.[15–20] Some researchers predicted the impact of the PEGylation site on the conformational stability of a protein using molecular dynamics (MD) simulations.[21,22] However, predictions were only verified on small peptides conjugated to short PEG chains.

The molecular mechanism of the effects of PEG addition on the protein properties remains unclear. The different impacts of PEGylation on the protein structure and/or stability may result, at least in part, from the approach used to carry out the PEGylation. Indeed, the size of PEG chains, the site of PEGylation and the linking chemistry may contribute to the consequences of PEG addition on the structure and/or stability of the protein. Therefore, the aim of this study was to compare the overall structure, thermodynamic stability, aggregation propensity, and proteolysis resistance of PEGylated AAT using PEGs of different lengths and structures, and different linking chemistries at two separated sites. The results obtained indicated that whatever the size/structure of the PEG and the site of conjugation, PEGylation had no effect on the structure and stability of the protein. On the other hand, the PEG size, PEG structure, and PEGylation site had a significant effect on the protection conferred to the protein against heat-induced aggregation and proteolysis. Conjugation of a 2-armed 40 kDa PEG to the cysteine232 residue resulted in the best resistance to heat-induced polymerization and proteolysis.

## 2 | RESULTS

### 2.1 | Chemical-induced unfolding transitions of AAT

According to the unfolding kinetic studies of AAT denaturation at different concentrations of GdmCl, the equilibrium is reached within 10 min. To ensure that the equilibrium is reached at all denaturant concentrations, all the GdmCl-induced unfolding samples were incubated at 25°C overnight before being analyzed.

The fluorescence spectrum of native AAT shows a wavelength of maximum fluorescence ($\lambda_{max}$) at around 330 nm (Figure 2a insert), indicating that the two tryptophan residues (Trp194 and Trp238) (or at least the one with the highest contribution) are relatively embedded within the core of the protein. Trp194 is at the top of β-sheet A and Trp238 on β-sheet B,[23] which is shown in Figure 1. With the increase of GdmCl concentration, the fluorescence intensity first increases and reaches its maximum at 2 M GdmCl; then it decreases as the GdmCl
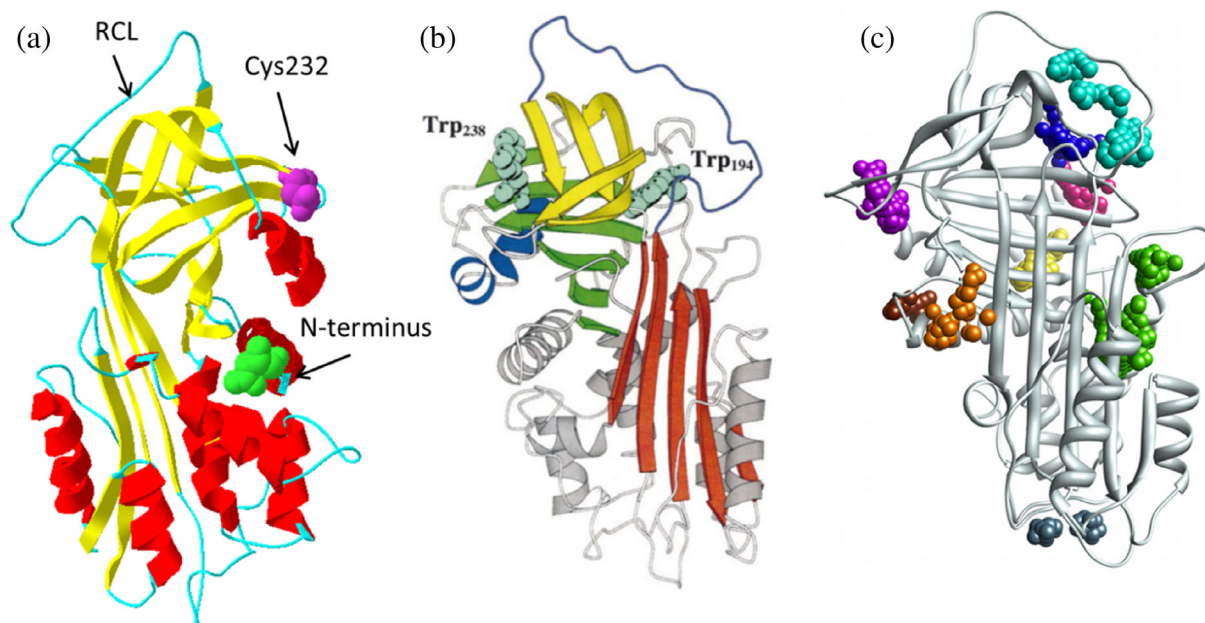
**FIGURE 1** (a) 3D structure of AAT (PDB: 2qug), generated by SWISS-MODEL.[24] The arrows indicate the reactive center loop (RCL) and the two PEGylation sites. (b) 3D structure of AAT with the two tryptophan residues highlighted. The A β-sheet is highlighted in red, the B β-sheet in green, and the C β-sheet in yellow. The RCL is in purple. (c) The nine top-ranking surface pockets identified by SiteMap on AAT. The green and the yellow ones are relatively hydrophobic. This figure is adapted from Tew et al.[25] and Patschull et al.[26]

concentration increases up to 6 M. As shown in Figure S1, the thermodynamic stability of the protein cannot be computed based on the unfolding curves monitored by the fluorescence intensity at a single wavelength (i.e., either at 330, 336 or 360 nm). The changes in wavelength at the maximum fluorescence ($\lambda_{max}$), exhibit, on the other hand, a clear double-sigmoid profile (Figure 2a) suggesting that the tertiary structure is denatured according to a three-state model (N ↔ I ↔ U). The first transition occurs between 0.7 and 1 M GdmCl, where the native protein (N) unfolds cooperatively into an intermediate state (I), followed by the second transition (from 1 to 4 M GdmCl) to the unfolded state (U). At 4–6 M GdmCl, the $\lambda_{max}$ reaches a plateau, indicating that the protein is fully unfolded. The values of the thermodynamic parameters are calculated assuming a three-state unfolding model and Equation (1) (Figure 2a and Table 1). AAT has a $\Delta G°_{NI(H2O)}$ of 13.7 ± 2.3 kJ·mol$^{-1}$ and $\Delta G°_{IU(H2O)}$ of 14.2 ± 0.7 kJ·mol$^{-1}$, and the mid-transition denaturant concentration of each transition ($C_m$) is 0.8 and 2.4 M, respectively.

Figure 2b insert shows the far UV-circular dichroism (CD) spectrum of AAT in the presence of different concentrations of GdmCl. The spectrum of native AAT shows negative maxima at 208 and 222 nm, indicating that AAT is an alpha helix-dominated protein, which is in agreement with the secondary content determined from X-ray crystallographic data: 33% in alpha-helices (9 alpha-helices), 28% in beta-sheet (3 beta-strands), and 39% in loops/unstructured.[27] In 6 M GdmCl, the CD signal is near to 0, indicating the full denaturation of the secondary structures. The unfolding transition monitored at 222 nm, exhibits a double-sigmoid profile (Figure 2b) suggesting that the secondary structure is also denatured according to a three-state model. Thus, the characteristic thermodynamic parameters are computed with the help of Equation (1), assuming a three-state unfolding model (Figure 2b and Table 1). The $\Delta G°_{NI(H2O)}$ is 16.3 ± 2.3 kJ·mol$^{-1}$ and $\Delta G°_{IU(H2O)}$ is 13.1 ± 0.8 kJ·mol$^{-1}$; these values are similar to those derived from fluorescent measurements within the error limit. The $C_m$ values of both transitions (0.8 ± 0.2 and 2.4 ± 0.1 M) are also similar to the one obtained from fluorescence measurements.

The ANS-bound fluorescence increases when ANS binds to the exposed hydrophobic clusters, which makes it a commonly used tool to detect the intermediate species exposing such clusters upon the unfolding of a protein.[28] Figure 2c insert shows the ANS-bound spectrum of AAT in the presence of various concentrations of GdmCl. ANS binds to AAT in its native state, suggesting the presence of hydrophobic clusters on the protein surface; this is confirmed by the X-ray structure of the protein (Figure 1). With the increase in GdmCl concentration, the ANS-bound fluorescence intensity at
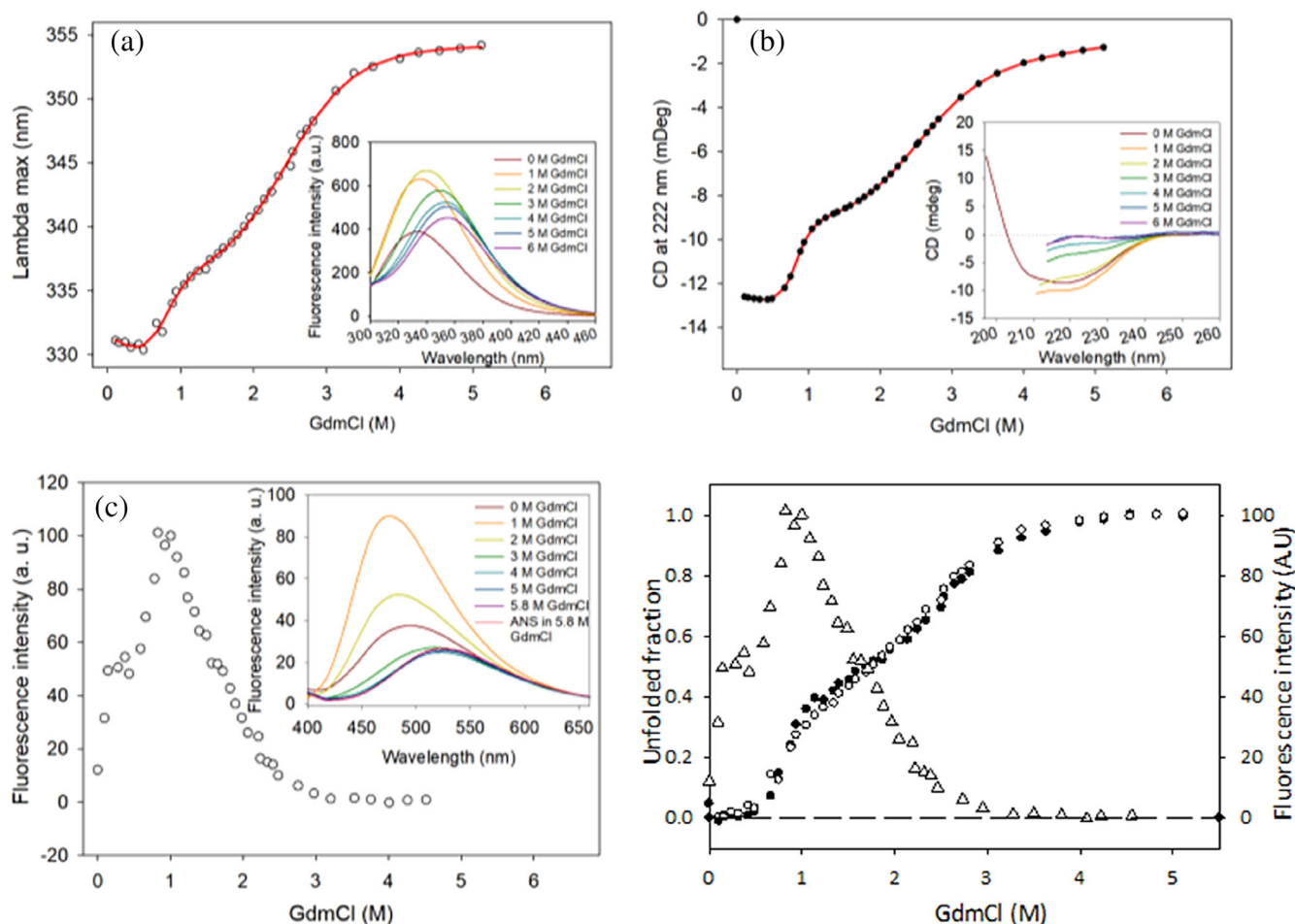
**FIGURE 2** (a) GdmCl-induced unfolding transition of AAT monitored by intrinsic fluorescence (i.e., by λmax). The insert shows the intrinsic fluorescence spectra of AAT in the presence of various concentrations of GdmCl. With the increase of GdmCl concentration, the fluorescence intensity first increased (0–2 M GdmCl) and then decreased (2–6 M GdmCl). A red shift (from approximately 330 to 355 nm) of the wavelength of maximum fluorescence is observed. (b) GdmCl unfolding transition of AAT monitored by far UV-CD. The insert shows the CD spectra of AAT in the presence of various concentrations of GdmCl. The CD signal decreased following a bimodal sigmoid. In 6 M GdmCl, the CD signal is near to 0, indicating the full denaturation of the secondary structures. In A and B, the lines represent the best fit to Equation (1) (c) GdmCl-induced unfolding transition monitored by ANS-bound fluorescence at 480 nm. The insert shows the ANS-bound fluorescence spectra of AAT in the presence of various concentrations of GdmCl. The red line shows the fluorescence spectrum of free ANS in 5.8 M GdmCl. ANS binds to AAT at native state, indicating the presence of hydrophobic clusters on the protein surface. With the increase of GdmCl concentration, the ANS-bound fluorescence intensity at 480 nm first increases then decreases, indicating first a higher exposure of hydrophobic patches followed by their unfolding. In the presence of >4 M GdmCl, the spectrum was superimposed with that of free ANS, indicating that the hydrophobic patches were fully unfolded. (d) Normalized transitions monitored by intrinsic fluorescence (empty circle) and far UV-CD (solid circle). The ANS-bound fluorescence intensity at 480 nm is also shown (empty triangle)

480 nm first increased (from 0 and 1 M in GmdCl), then it decreased to near 0. These results suggest that the intermediate formed in the presence of 1 M GdmCl is associated with the exposure of a hydrophobic cluster.

Figure 2d shows the normalized transitions monitored by intrinsic fluorescence, far UV-CD, and ANS-bound fluorescence. The normalized unfolding transitions obtained by far UV-CD and intrinsic fluorescence coincide indicating that the secondary and the tertiary structures of the protein unfold cooperatively.

## 2.2 | Effect of PEGylation on structure and stability of AAT

### 2.2.1 | Secondary and tertiary structures

Figure 3a shows the intrinsic fluorescence spectra of AAT and PEGylated AAT in the native and unfolded states (i.e., in 6.9 M GdmCl). The spectra of the different PEGylated AAT exhibit the same $\lambda_{max}$ as AAT but show significantly higher fluorescence intensity in their native state.

**TABLE 1** Thermodynamic parameters derived from the GdmCl-induced unfolding transition of AAT and PEG-AAT, based on intrinsic fluorescence measurement (i.e., changes in wavelength at the maximum fluorescence) and far UV-CD (at 222 nm). The transitions were analyzed assuming a three-state unfolding model.

| Protein | $\Delta G°_{NI(H2O)}$ (kJ·mol$^{-1}$) | $m_{NI}$ (kJ·mol$^{-1}$·M$^{-1}$) | $Cm_{NI}$ (M) | $\Delta G°_{IU(H2O)}$ (kJ·mol$^{-1}$) | $m_{IU}$ (kJ·mol$^{-1}$·M$^{-1}$) | $Cm_{IU}$ (M) |
|---|---|---|---|---|---|---|
| **Intrinsic fluorescence** | | | | | | |
| WT AAT | 13.7 ± 2.3 | 17.4 ± 2.4 | 0.8 ± 0.2 | 14.2 ± 0.7 | 5.9 ± 0.3 | 2.4 ± 0.1 |
| Linear PEGMA30k-AAT | 13.5 ± 2.9 | 16.7 ± 3.0 | 0.8 ± 0.3 | 14.2 ± 0.9 | 6.0 ± 0.4 | 2.4 ± 0.1 |
| Linear PEGMA40k-AAT | 15.6 ± 2.6 | 19.7 ± 2.9 | 0.8 ± 0.2 | 14.3 ± 0.8 | 6.2 ± 0.3 | 2.3 ± 0.1 |
| 2-armed PEGMA40k-AAT | 11.9 ± 3.1 | 15.5 ± 3.1 | 0.8 ± 0.3 | 13.7 ± 1.4 | 5.8 ± 0.6 | 2.4 ± 0.2 |
| 2-armed PEGAL40k-AAT | 13.0 ± 3.0 | 17.5 ± 3.3 | 0.7 ± 0.3 | 13.3 ± 0.8 | 5.6 ± 0.4 | 2.4 ± 0.1 |
| **Far UV-CD** | | | | | | |
| WT AAT | 16.3 ± 2.3 | 20.4 ± 2.3 | 0.8 ± 0.2 | 13.1 ± 0.8 | 5.5 ± 0.5 | 2.4 ± 0.1 |
| Linear PEGMA30k-AAT | 13.1 ± 2.5 | 15.5 ± 2.7 | 0.8 ± 0.3 | 14.4 ± 0.9 | 6.0 ± 0.6 | 2.4 ± 0.1 |
| Linear PEGMA40k-AAT | 15.6 ± 1.9 | 17.9 ± 1.9 | 0.9 ± 0.2 | 13.2 ± 1.8 | 5.4 ± 0.6 | 2.5 ± 0.2 |
| 2-armed PEGMA40k-AAT | 14.5 ± 3.7 | 15.9 ± 3.2 | 0.9 ± 0.3 | 14.9 ± 0.9 | 6.0 ± 0.3 | 2.5 ± 0.2 |
| 2-armed PEGAL40k-AAT | 13.0 ± 2.7 | 16.0 ± 3.2 | 0.8 ± 0.3 | 13.0 ± 0.9 | 5.6 ± 0.4 | 2.3 ± 0.1 |
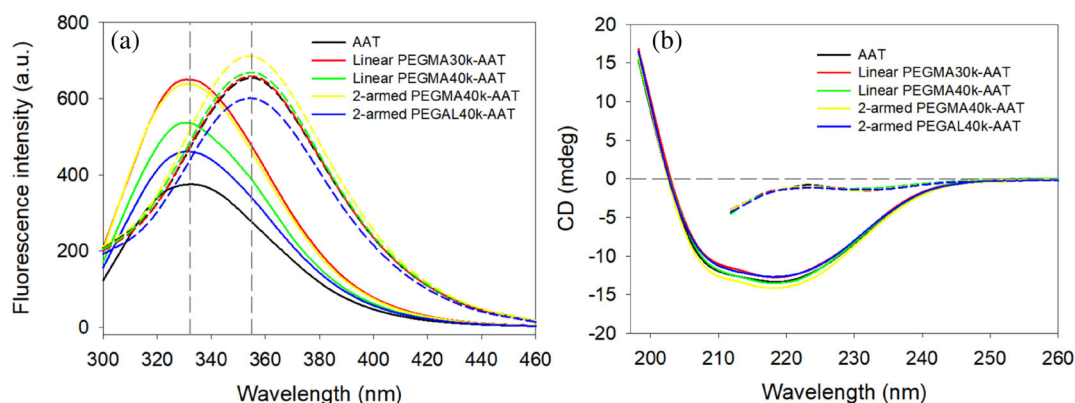


**FIGURE 3** Fluorescence and far UV-CD spectra of AAT and PEGylated AAT in the absence of GdmCl (solid lines) and in the presence of 6.9 M GdmCl (dashed lines). (a) Intrinsic fluorescence spectra. The wavelength of maximum fluorescence of PEGylated AAT in the native state is ~330 nm, while in the denatured state (in the presence of 6.9 M GdmCl) is ~355 nm, indicating the full denaturation of the tertiary structure. (b) Far UV-CD spectra. AAT and PEG-AAT share an identical CD spectrum, indicating that the secondary structure is not modified upon PEGylation

The increase in fluorescence intensity is observed whether the PEG moiety is attached via the W128-closed-by cysteine 232 or the farther N-terminus. Moreover, there is no obvious correlation between the amplitude of the increase in fluorescence intensity and the length of the PEG. In the presence of 6.9 M GdmCl, the spectra of PEGylated AAT are similar to that of AAT, which indicates the full denaturation of the tertiary structures of the PEGylated proteins.

Figure 3b shows the far-UV CD spectra of unmodified and PEGylated AAT. The spectra of PEGylated AAT show the same signal and shape, which confirms that after PEGylation, there are no significant changes in the secondary structure whatever the position and the length

of the PEG. In the presence of 6.9 M GdmCl, the CD signals of all the proteins are near 0, indicating that all the proteins are fully unfolded.

## 2.2.2 | Thermodynamic stability

Figure 4a shows the normalized GdmCl unfolding transition of AAT and PEGylated protein monitored by intrinsic fluorescence. Whatever the length and the position of the PEG chain, PEGylated AAT unfolds according to a three-state transition. The unfolding curves of PEGylated AAT are superimposed with that of unmodified AAT,
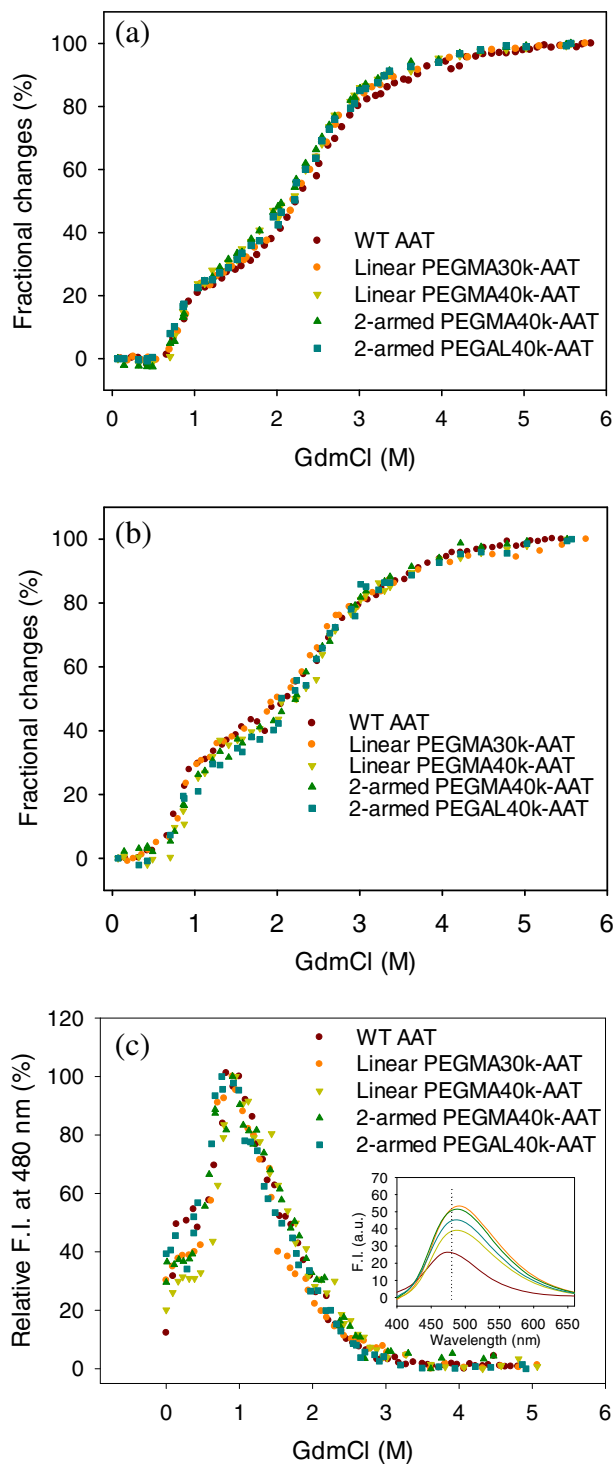
**FIGURE 4** GdmCl-induced transitions shown as fractional changes in the signal of: intrinsic fluorescence (λmax) (a), far UV-CD signal at 222 nm (b) and ANS-bound fluorescence intensity at 480 nm (c). The insert in (c) shows the ANS-bound fluorescence spectra of AAT and PEG-AAT in the absence of GdmCl. The colors of the spectra are the same as in (c). AAT and PEG-AAT unfold in a three-state transition. The unfolding curves of PEG-AAT are superimposed with that of AAT, indicating that the PEGylation does not affect the stability of AAT

indicating that PEGylation does not significantly affect the thermodynamic stability of the protein. A non-linear fit is performed using Equation (1) to all the non-normalized transition curves, which results in similar thermodynamic parameters within experimental errors for unmodified and PEGylated proteins (Table 1).

As monitored by intrinsic fluorescence, AAT has a $\Delta G°(H_2O)$ value of $13.7 \pm 2.3$ and $14.2 \pm 0.7$ kJ·mol$^{-1}$, and the $C_m$ value of $0.8 \pm 0.2$ and $2.4 \pm 0.1$ M for the first and second transitions, respectively. As shown in Table 1, PEGylation did not change the thermodynamic parameters of AAT significantly.

The unfolding transitions were also monitored by the CD signal at 222 nm. Figure 4b displays the normalized unfolding transitions. The transition curves of PEGylated AAT are superimposed with that of AAT, suggesting that the PEGylation does not affect the unfolding of the secondary structure of AAT. A satisfactory fit was obtained using Equation (1) to each transition curve before normalization. The analysis gives a similar $\Delta G°(H_2O)$ value of AAT of $16.3 \pm 2.3$ and $13.1 \pm 0.8$ kJ·mol$^{-1}$ (Table 1) and $C_m$ value of $0.8 \pm 0.2$ and $2.4 \pm 0.1$ M for the first and second transitions. PEG-AAT showed similar thermodynamic parameters monitored by far UV-CD (Table 1), indicating that PEGylation did not drastically alter the stability of AAT towards GdmCl-induced unfolding.

As shown in Figure 2c, the transitions of PEGylated proteins monitored by ANS extrinsic fluorescence are superimposed with that of AAT, with the same maxima at 1 M and decreasing signal from 1 to 3 M GdmCl, supporting the results from intrinsic fluorescence and far-UV CD measurements that PEGylation did not influence the stability of AAT to GdmCl-induced unfolding.

The activity of the samples refolded from GdmCl-induced unfolded protein (6 M) were determined by measuring their ability to inhibit human sputum elastase (hNE) activity (Figure S3). The refolded samples showed similar hNE inhibition capacity as the native proteins. This indicates that the GdmCl-induced unfolding of AAT is largely reversible and that the PEGylation does not interfere with the refolding process.

## 2.3 | Heat-induced unfolding transitions

### 2.3.1 | Intrinsic fluorescence and far UV-CD spectra of AAT

To determine the appropriate wavelength to monitor thermal-induced denaturation of AAT and PEGylated AAT, the fluorescence and far-UV CD spectra of AAT at

**FIGURE 5** (a) Intrinsic fluorescence spectrum of unmodified AAT at different temperatures; (b) far UV-CD spectrum of AAT at different temperatures
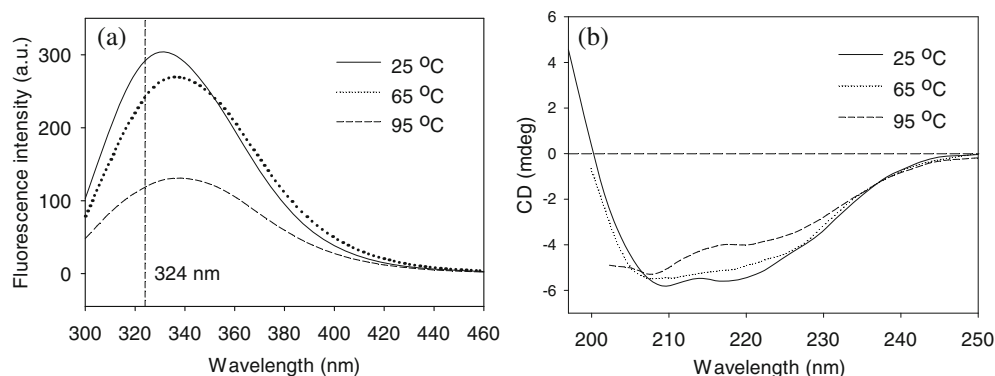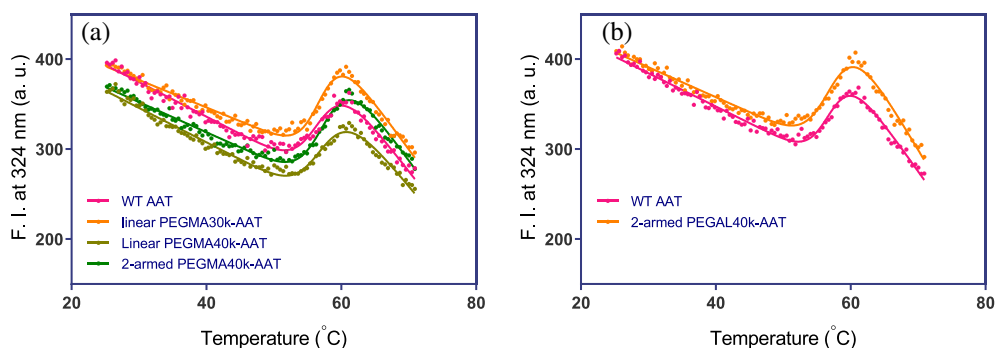


**FIGURE 6** Thermal-induced transitions of AAT and PEG-AAT, followed by the changes of intrinsic fluorescence at 324 nm (a, b). The lines represent the best fit to Equation (2). FI, fluorescence intensity



different temperatures were recorded (Figure 5). Panel (a) shows the fluorescence spectrum of AAT at 25°C (solid line), 65°C (dotted line), and 95°C (dashed line). At 65°C, the fluorescence maximum ($\lambda_{max}$) shifted to higher wavelength (i.e., 340 nm), with a slight decrease in fluorescence intensity. At 95°C, the fluorescence intensity dropped drastically; the $\lambda_{max}$, however, barely changed. The most significant difference in the fluorescence intensity occurs at around 324 nm; therefore, this wavelength was chosen to monitor the thermal unfolding of the proteins. In the far-UV CD spectra (panel (b)), the CD signal decreased with increasing the temperature, especially for the negative minimum at 222 nm. However, at 95°C, the spectrum suggests that a significant amount of secondary structure is still present. When AAT is fully denatured, the $\lambda_{max}$ in fluorescence shifts to approximately 355 nm and the CD signal is nearly 0, which is neither the case with AAT at high temperature. This may suggest that at high temperature, AAT is not completely denatured. This is however not likely the case since the apparent $T_m$ observed was around 57°C (see below). Therefore, it is more likely that the unfolded protein had significantly aggregated. The heated AAT shows no elastase inhibition activity (Figure S3), which supports that the thermal denaturation of AAT is not reversible most likely due to the aggregation of the protein. Thus, transition monitored by intrinsic fluorescence will only allow to grossly evaluate if the PEGylation has an effect on the thermostability through the $T_m^{app}$ value.

### 2.3.2 | Effect of PEGylation on the thermal stability of AAT

Figure 6a,b shows the thermal transitions of the unmodified and PEGylated AAT monitored by intrinsic fluorescence at 324 nm. All the transitions show a linear decrease in fluorescence intensity from 25 to 50°C, which corresponds to the pre-transition baseline. With the continuous increase of the temperature, the fluorescence intensity increased and peaked at around 60°C. From 60 to 70°C, the fluorescence intensity linearly decreased and corresponded to the post-transition baseline. The transition curves monitored by intrinsic fluorescence were fitted using Equation (2). As shown in Table 2, AAT and PEG-AAT showed a similar mid-transition temperature ($T_m^{app}$) around 57–58°C.

Figure 7 shows the changes of the averaged hydrodynamic size of unmodified and PEGylated AAT with the increase in temperature. The hydrodynamic diameter of AAT and PEGylated AAT at different temperatures were measured by Malvern Zetasizer Ultra. AAT had a size of $6.2 \pm 0.1$ nm at 25°C, which was unchanged until 55°C. The size of heated protein increased gradually and reached $16.1 \pm 0.9$ nm from 55 to 97°C, indicating the formation of aggregates. The aggregates started to accumulate at around 55°C, which corresponded roughly to the $T_m^{app}$ derived from the thermal unfolding experiments monitored by intrinsic fluorescence. This observation further supports that the irreversibility of the heat-

induced denaturation is due to the aggregation of unfolded protein. The normalized data show that the relative size of AAT significantly increased starting from 55°C, while for PEG-AAT the increase started at around 60°C. Since the Tm$^{app}$ measured by far UV-CD is similar whether the protein is PEGylated or not, these results suggest that the PEG moiety act by decreasing the

intermolecular interactions between unfolded molecules. In addition, at 95°C, the size of PEG-AAT was approximately 1.6-fold larger than the native monomers. While for AAT, the size almost tripled at 95°C. The inhibition of the aggregation is similar whatever the PEGylation site and length.

The effect of PEGylation on the irreversible aggregation of AAT was also monitored by SEC following treatment at 70°C for 1 h. The samples were left to return to RT before analysis. Insoluble aggregates in thermally-denatured samples were first removed by filtering through a 0.22-μm cut-off membrane. The soluble aggregates were quantified by SEC. As shown in Figure 8 and Figure S2, the content of AAT and PEG-AAT remaining in solution was determined by analyzing the peak area percentage of the chromatograms. Both AAT and PEG-AAT show an increase of aggregation after thermal denaturation. The chromatogram of AAT after denaturation shows 32.7% of the native monomers (the peak at 16 ml), which represents a 60% decrease compared to the control sample. Besides the monomers, there are several peaks eluting earlier than the monomer, which correspond to aggregated species (54.7%). Worth mentioning that the

**TABLE 2** Apparent mid-transition temperature ($T_m{}^{app}$) of AAT and PEG-AAT during thermal denaturation

| Proteins | $T_m{}^{app}$ from intrinsic fluorescence measurements (°C) |
|---|---|
| AAT | $57.2 \pm 0.3$ |
| Linear PEGMA30k-AAT | $57.3 \pm 0.2$ |
| Linear PEGMA40k-AAT | $57.8 \pm 0.3$ |
| 2-armed PEGMA40k-AAT | $58.1 \pm 0.2$ |
| 2-armed PEGAL40k-AAT | $57.8 \pm 0.3$ |

*Note*: Thermal induced unfolding of AAT and PEGylated AAT was followed by intrinsic fluorescence at 324 nm. The transition curves were fitted using Equation (2) by GraphPad Prism 8.
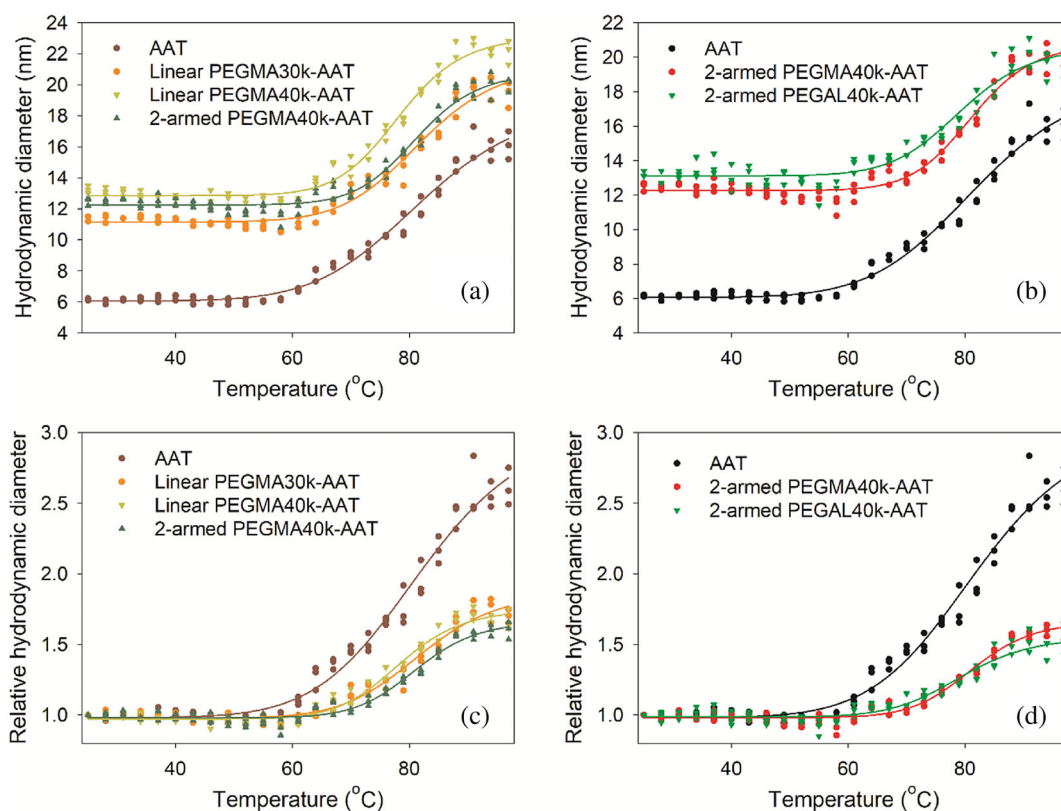


**FIGURE 7** Heat-induced aggregation of AAT and PEG-AAT monitored by DLS. (a) AAT and thiol PEGylated AAT. (b) AAT, 2-armed PEGMA40k-AAT and 2-armed PEGAL40k-AAT. (c, d) show the normalized data from (a, b). PEGylated AAT has larger hydrodynamic diameter than AAT. As the temperature increases, the size of AAT and PEG-AAT stayed unchanged until 55°C, followed by a gradual increase. DLS, dynamic light scattering
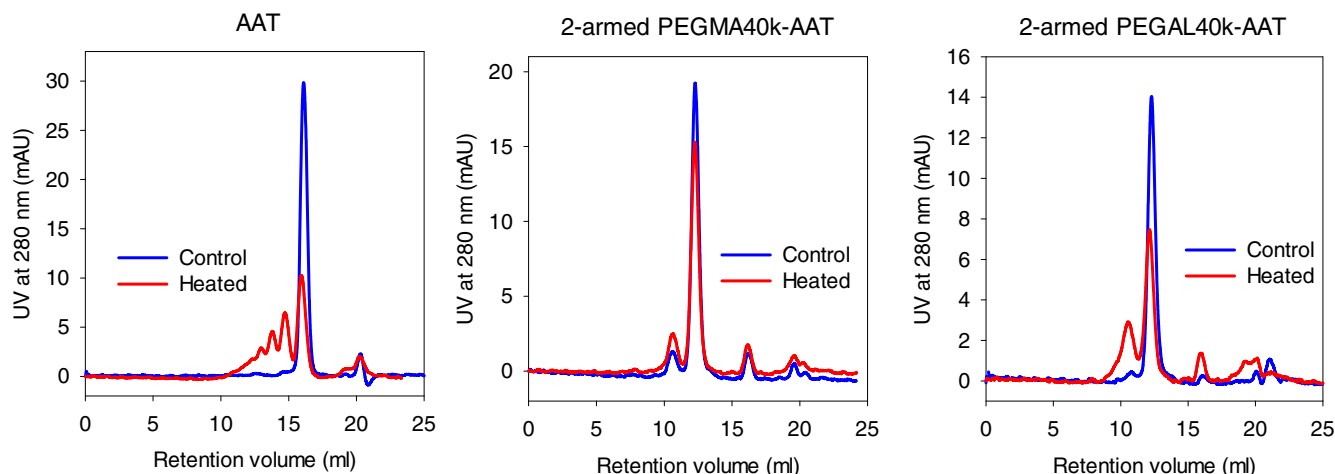
**FIGURE 8** Size exclusion chromatograms of AAT and PEG-AAT after heat treatment (70°C, 1 h). The control samples at the same concentration were kept at room temperature for 1 h. The large insoluble aggregates were primarily removed by filtration through 0.22 µm cut-off membrane. PEG-AAT showed less aggregates after heating than AAT. Thiol PEGylated AAT has better resistance to heat-induced aggregation than N-terminal PEGylated AAT

aggregates measured by dynamic light scattering show the most abundant entities at 23 nm, which would remain in the solution after filtration through 0.22 µm cut-off membrane. The non-filtered heated samples show increased UV absorbance at 350 nm, indicating the presence of insoluble aggregates, which were removed by filtration. Following N-terminal PEGylation with 2-armed 40 kDa PEG-AL, the aggregation content was significantly decreased (only 25.7%). Following thiol PEGylation, the linear PEG-MA modified AAT showed an even lower content of aggregates. Two-armed PEGMA40k-AAT showed the best resistance to polymerization, as there was only 13.5% of the aggregates. The remaining activity of the heated samples was determined by an elastase inhibition assay. As shown in Figure S3, the hNE activity was completely inhibited by native unmodified or PEGylated AAT at a hNE:AAT molar ratio 1:1, while it was not inhibited at all by heated AAT products. The heated PEGylated AAT did not therefore present any hNE inhibition capacity despite the fact that heat-induced aggregation was reduced. This demonstrated that the activity of unmodified and PEGylated AAT was fully and irreversibly lost after heating.

## 2.4 | Stability to proteolysis

AAT is a serine protease inhibitor, which can inhibit a wide range of proteases, including the serine protease family and cysteine proteases family.[29] Matrix metalloproteinases (MMPs) were reported to digest AAT without being directly inhibited by AAT.[30] This family of proteases is produced by inflammatory cells (neutrophils and
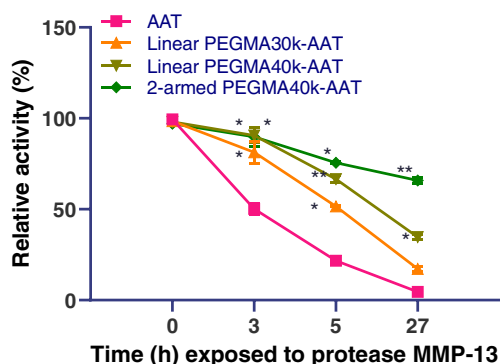


**FIGURE 9** The hNE inhibition activity (AAT or PEG-AAT: hNE molar ratio was 1:1) of AAT and PEG-AAT after exposure to the protease MMP-13 for 3, 5, and 27 hr. With the exposure to MMP-13, AAT loses more rapidly its hNE inhibitory activity compared with PEG-AAT. Two-armed PEGMA40k-AAT maintains >65% of the activity after 27 hr exposure. Statistical differences were analyzed by fitting a mixed model in GraphPad Prism 8. The star marks on top of each bar indicate significant difference (*$p < .05$, **$p < .01$) that bar to AAT

alveolar macrophages). The expression of matrix metalloproteinase 13 (MMP-13) is increased in the lungs of COPD patients.[31] Therefore, it is of interest to investigate the resistance of AAT and PEG-AAT to this protease. As shown in Figure 9, after exposure to MMP-13 for 3, 5, and 27 hr, AAT and PEG-AAT show activity loss as the time of exposure increases. AAT is vulnerable to MMP-13 proteolysis; it indeed loses approximately 50% of its capacity to inhibit hNE after 3-hr exposure to MMP-13 and it loses all its activity after 27 hours. PEG-AAT shows stronger resistance to MMP-13. At 3 hours, all PEG-AAT

loose less than 20% of their activity. With longer exposure, AAT conjugated to 2-armed PEG molecule shows lower activity loss than the ones conjugated to linear PEG. After 27-hour exposure, two-armed PEG-AAT still preserves $66 \pm 2\%$ of activity. These results highlight that PEGylation significantly improves the proteolytic resistance of AAT. This proteolytic resistance is enhanced by increasing the PEG molecular weight or changing the PEG structure; indeed 2-armed PEG confers the best enhancement of proteolytic resistance.

# 3 | DISCUSSION

In this study, the overall structure, thermodynamic stability, aggregation propensity, and proteolysis resistance of PEGylated versions of AAT were compared to unmodified AAT. The PEG molecules used were linear 30 kDa, linear 40 kDa, and 2-armed 40 kDa. These PEGs were selected as they are applied in clinically-approved PEGylated proteins; they represent the largest sizes used and have a size comparable to that of AAT. We chose to investigate N-terminal PEGylation of AAT[32] as it has not been previously reported. Although thiol PEGylation has been previously investigated by Cantin et al., the authors did not mention whether the disulfide bridge between the Cys232 and the cysteine cap was reduced before the PEGylation.[33] Therefore, we also chose this PEGylation site and chemistry to confirm and complete Cantin's work.

## 3.1 | Effects of PEGylation on the secondary and tertiary structures of AAT

The far-UV CD spectrum of unmodified and PEGylated AAT shows that the secondary structure of AAT is not significantly affected by both thiol and N-terminal PEGylation. Among numerous studies concerning PEGylation of a protein, an alteration of protein secondary structure was seen only in the cases where a large PEG was used, which often combined with some loss of activity. For instance, Chiu et al. found that the conjugation of a 20 kDa PEG to trypsin caused a significant loss in its secondary structure, especially α-helices, and in its biological activity.[34] In this case, however, the reaction was not site-selective and there were multiple PEGylation sites. In the cases of mono-PEGylation to a selective PEGylation site, PEGylation usually does not alter the protein secondary structure.[9,17,19,35,36] As for the tertiary structure, the PEGylated AAT showed the same $\lambda_{max}$ in fluorescence spectra as that of AAT, suggesting that there were no significant structural changes in the

environment of the tryptophan residues, and thus of the tertiary structure of the protein upon PEGylation. In addition, the ability of AAT to inhibit human neutrophil elastase was fully preserved after PEGylation, as previously described.[32] An increase in intrinsic fluorescence intensity is however observed for the PEGylated AAT compared to AAT. With thiol PEGylation, the linear PEGMA30k-AAT and 2-armed PEGMA40k-AAT showed higher fluorescence intensity than the linear PEGMA40k-AAT. In the native state, the fluorescence of the tryptophan residues may be quenched by the disulfide bond between Cys232 and the cysteine cap.[37] When conjugating a PEG-maleimide to Cys232, the disulfide bond between Cys232 to the additional cysteine cap no longer exists, thus its quenching should not be present anymore, causing the increase of the intrinsic fluorescence intensity. Other studies show that PEGylation can decrease the protein intrinsic fluorescence[38] or has no effect.[39–41] The decrease of intrinsic fluorescence in β-lactoglobulin (β-LG) after PEGylation was explained as a combined action of the shielding effect of the PEG chain and the exposure of the Trp residues to the solvent upon PEGylation.[38] In the case of granulocyte colony-stimulating factor (G-CSF), PEGylation at two different sites (Lys41 and Gln135) resulted in unchanged or increased intrinsic fluorescence intensity, respectively.[38]

PEGylated AAT displays the same biological activity as AAT, indicating that PEGylation does not affect the structure of the most important part of this protein, the reaction center loop (RCL).[32] These results are in line with Zhu et al.[42] and Cantin et al.[33] It is reported from several studies that PEGylation does not alter the tertiary structure of a protein substantially. Plesner et al. reported the PEGylation of bovine serum albumin and recombinant human factor VIIa, respectively, and their results showed identical near UV-CD spectra of unmodified and PEGylated proteins.[36] Rodríguez-Martínez et al. reported that no major spectral changes were observed as a result of PEGylation of α-chymotrypsin.[17] Guichard et al.[35] demonstrated that mono-PEGylated recombinant human deoxyribonuclease I (rhDNase) shared the same intrinsic tryptophan fluorescence spectrum as the unmodified rhDNase, in which case the PEGylation site was the N-terminal residue, which is distant from all four tryptophan residues.

## 3.2 | Effects of PEGylation on thermodynamic stability

The thermodynamic stability of AAT and PEGylated AAT was determined by intrinsic fluorescence, far-UV CD, and ANS-bound fluorescence measurements in the

presence of increasing concentrations in GdmCl. The reversibility of GdmCl-induced unfolding of AAT and PEGylated AAT was established by an hNE inhibition assay of refolded AAT samples.[36] After refolding, the hNE inhibition capacity of AAT and PEGylated AAT was fully regained. Both fluorescence and far-UV CD data show that AAT and PEGylated AAT unfold via a three-state transition (N ⇋ I ⇋ U, where N represents the native state, I the intermediate state, and U the unfolded state), with the $C_m$ value around 0.8 and 2.4 M, respectively, which is in good agreement with previous reports.[25,43–45] However, the ΔG values from different studies vary. Krishnan et al. reported both $\Delta G^\circ_{NI(H_2O)}$ and $\Delta G^\circ_{IU(H_2O)}$ as 16.7 kJ·mol$^{-1}$,[44] while in the study of Tew et al., $\Delta G^\circ_{NI(H_2O)}$ was 19.7 kJ·mol$^{-1}$ and $\Delta G^\circ_{IU(H_2O)}$ was 25.5 kJ·mol$^{-1}$.[25] Hence, the concentration of GdmCl at which the intermediate is formed varies from 1.0 to 1.5 M.[44,47] In these two studies, the unfolding curves were monitored by far-UV CD. Our data ($\Delta G^\circ_{NI(H_2O)}$ as 16.3 ± 2.3 kJ·mol$^{-1}$ and $\Delta G^\circ_{IU(H_2O)}$ as 13.1.0 ± 2.4 kJ·mol$^{-1}$) are in better agreement with Krishnan et al. The superimposition of transitions monitored by fluorescence and far-UV CD indicates the simultaneous denaturation of the secondary and tertiary structures for unmodified and PEGylated AAT. This denaturation profile suggests that the protein behaves as two structurally independent domains that cooperatively unfold independently. It was reported that the intermediate of AAT formed upon chemical unfolding involved only the A and C β-sheet, while the B β-sheet was intact, which corresponds to our proposition that the protein unfolds as two domains independently. For example, Tew et al. show that the A β-sheet undergoes a conformational change resulting in the increased exposure of Trp194 to solvent in 3.5 M urea, while no change in the B β-sheet (where Trp238 is located) is observed.[25] Similarly, Krishnan et al.[44] demonstrate that the chemical unfolding intermediate of AAT contains an intact B β-sheet. Tsutsui et al., using H/D exchange experiments, suggested however that the unfolding of AAT involved a cooperative transition to a molten globule form, followed by a non-cooperative transition to a random-coil form as more guanidine was added. Thus, the entire AAT molecule consists of one cooperative structural unit rather than multiple structural domains with different stabilities.[43]

For all proteins investigated in the present study, the transition curves monitored by ANS-bound fluorescence show an increase in fluorescence intensity up to around 1 M GdmCl, followed by a decrease in intensity at higher GdmCl concentrations. The increase of ANS-bound fluorescence upon the first transition might be due to the exposure of a hydrophobic cluster at the interface of the two domains. The cluster is likely to be denatured at higher denaturant concentrations.

The free energy of each protein was obtained by adjusting the experimental transition curves by Equation (1) (Table 1). All the proteins share a similar $\Delta G^\circ(H_2O)$ value within the experimental error (12–16 kJ·mol$^{-1}$). The $\Delta G^\circ(H_2O)$ and $C_m$ values for the first and second transitions of AAT did not change drastically after PEGylation. These results highlight that the conformational stability of AAT towards chemical denaturant is not significantly altered upon PEGylation.

García-Arellano et al.[18] reported that the thermodynamic stability of Cytochrome C (12.4 kDa) decreased after conjugating a 5 kDa PEG: the $\Delta G^\circ(H_2O)$ of PEGylated Cytochrome was 7.3 kJ·mol$^{-1}$, while that of the unmodified protein was 25.1 kJ·mol$^{-1}$ Similarly, Sorret et al.[48] found that the $\Delta G^\circ(H_2O)$ of recombinant human interleukin-1 receptor antagonist (rhIL-1ra), a 17 kDa cytokine inhibitor, decreased by 22.6 kJ·mol$^{-1}$ upon conjugation to a 20 kDa PEG chain.

Interestingly, as shown in Figure 3, ANS binds to AAT and PEGylated AAT in the native state. Elliott et al.[49] also observed ANS-binding to native AAT. The native state of AAT is meta-stable, which does not correspond to the most stable conformation that its sequence can adopt.[50,51] Indeed, upon binding to its cognate protease, AAT undergoes a massive conformational change, in which the RCL inserts into β-sheet A, becoming the sixth strand. The resulting conformation is more stable than the initial native structure.[46,52] Inspecting the crystal structure of AAT, a hydrophobic pocket that is lined by two of A β-sheets and α-helices D and E (Figure 1, purple area on the right) is observed,[53] which plays a crucial role in the polymerization of misfolded AAT.[54,55] Another hydrophobic surface was detected as shown in Figure 1 (purple area on the left), where locates one of the tryptophan residues (Trp194). These hydrophobic areas are likely the binding region for ANS.

## 3.3 | Effect of PEGylation on thermal stability

The apparent mid-transition temperatures ($T_m^{app}$) of AAT and PEG-AAT monitored by intrinsic fluorescence intensity at 324 nm are similar (∼57.6 ± 0.3°C). AAT and PEGylated AAT did not recover any activity after heat treatment. The DLS and SEC analyses of the denatured samples proved that the thermal denaturation of unmodified and PEGylated AAT is associated with significant aggregation. Previous studies have shown that heat-

induced denaturation of AAT is a concentration-dependent aggregation process.[56,57]

The results of size distribution data illustrate that the polymerization starts from around 50 to 55°C for AAT and 60 to 65°C for PEG-AAT. This suggests that aggregation occurs following heat denaturation possibly from unfolded species. Haq et al. have shown that an AAT intermediate is formed upon heating between 25 and 95°C.[58] The PEG-AAT has a lower tendency to aggregate indicating that PEGylation prevents intermolecular interactions as previously reported by Roque et al.[59] They demonstrated that the conjugation of two 30 kDa PEG-maleimide to a monoclonal antibody fragment (Fab′) protected it against the formation of heat-induced large aggregates and precipitation, possibly by sterically hindering intermolecular association between partially unfolded protein molecules.[59] N-terminal PEGylation of granulocyte colony-stimulating factor (GCSF) with a 20 kDa PEG prevents protein precipitation, and slows the aggregation rate.[60] However, PEG-maleimide conjugation to the Cys17 of GCSF, enhances the tendency of GCSF to aggregate.[61] These results suggest that the PEGylation site has a strong influence on protein aggregation.

The results of the SEC analysis also support that the effects of PEGylation on the properties of the protein are site-specific in the case of AAT. AAT shows weak resistance to thermal-induced aggregation. Among all the PEGylated protein, 2-armed PEGMA40k-AAT presents the highest content in monomers after thermal denaturation, with a loss of only 15% of monomeric proteins. Although at least 30% of the protein molecules remained monomeric after thermal denaturation, the hNE inhibition assay showed the complete loss of activity in all samples. This indicates that after heating, either polymerized or monomeric AAT are inactive, which is in agreement with the findings from Persson et al.[62] and Lomas et al.[57] These authors indeed reported that when heating at high temperature (i.e., 65–68°C), the uncleaved RCL can be stably incorporated into the A β-sheet, which is characterized as latent AAT. Latent AAT is inactive[44] but more resistant to heat-induced polymerization.[63,64] Therefore, it is likely that the monomeric species present in the heat-treated sample are latent AAT. In our case, thiol PEGylated AAT showed better resistance to heat-induced polymerization than N-terminal PEGylated AAT. This observation suggests that thiol-PEGylation favors the formation of the latent state of AAT upon heating, although this should be further verified experimentally. In the case of GCSF, N-terminal PEGylated GCSF is more stable than the thiol-PEGylated one.[60,61] This indicates that the influence of the PEGylation site on protein thermal stability differs between proteins and that it is difficult to predict the effects for a given protein.

## 3.4 | Effect of PEGylation on the stability toward proteolysis

PEGylation is often used to increase the stability of a therapeutic protein to proteolysis. Zhang et al. demonstrated that the conjugation of 2–10 kDa PEG on lysine residue of fibronectin enhanced its resistance to proteolysis.[65] Similar effect was reported with fibronectin PEGylated on a cysteine residue by thiol PEGylation.[66] Danial et al. showed that conjugating a 2 kDa PEG to the peptides derived from the HR1 or HR2 regions of the HIV-1 envelope glycoprotein gp41 resulted in an increase of 3.4-fold in degradation half-life against trypsin.[67] However, the mechanism behind this is not yet thoroughly investigated. The prominent explanation of the proteolytic protection conferred by PEG is the steric shielding effect, which impedes the access of proteases towards the protein.[10] Nevertheless, this shielding effect can sometimes result in the loss of affinity for its physiological partners or of its activity. Growth hormone antagonist (GHA), a 22 kDa protein, loses its binding affinity after conjugating to a 40 kDa PEG at the N-terminus.[11] Pegaptanib®, the PEGylated aptamer against vascular endothelial growth factor (VEGF) with a 2-armed 40 kDa PEG, preserves only 25% of the in vitro binding affinity, compared with its unconjugated counterpart.[12] Nonetheless, the tremendous increase in half-life (9 days for Pegaptanib® versus 30 min for unconjugated anti-VEGF) offsets the loss of activity, leading to an overall better therapeutic value. Similarly, Pegasys®, a PEGylated interferon-α-2a, preserved only 7% of the in vitro activity but showed an excellent in vivo efficacy.[12] Our results showed that two-armed PEGMA40k-AAT has the most enhanced resistance to proteolysis. Moreover, the reduction of proteolysis is achieved without compromising the biological activity.

## 4 | CONCLUSIONS

The main result of this systematic analysis of the effects of PEGylation on AAT stability is that PEGylated ATT is less sensitive to proteolysis than unconjugated AAT while PEGylation has no effect on the structure and thermodynamic stability of the protein. The protection towards the MMP-13 protease is the highest upon thiol-PEGylation with a 2-armed 40 kDa PEG. Therefore, 2-armed PEGMA40-AAT could be a promising candidate to prolong the half-life of AAT after its infusion or inhalation in AAT-deficient patients and therefore decrease the frequency of administrations. These improvements will both decrease the cost of treatment and increase the patient compliance. Further studies using relevant rodent models

(i.e., AAT-deficient mice or animals with COPD) are however needed to confirm these results in vivo.

# 5 | MATERIALS AND METHODS

## 5.1 | Materials

The wild-type AAT was purified by size exclusion chromatography (SEC) from a commercial human AAT product – Pulmolast® (Lamepro, Breda, The Netherlands). The linear 30 kDa, 40 kDa, and 2-armed 40 kDa PEG-maleimide and linear 30 kDa, 40 kDa, and 2-armed 40 kDa PEG-aldehyde were purchased from NOF Europe GmbH (Frankfurt, Germany). The hNE and its substrate N-Succinyl-Ala-Ala-Ala-pNitroanilide were purchased from Elastin Products Company, Inc. (Owensville, MO). The other reagents, if not mentioned specifically, were from Sigma-Aldrich, Inc. (Overijse, Belgium).

## 5.2 | Production and purification of mono-PEGylated AAT

The synthesis of mono-PEGylated AAT was as described previously.[32] Briefly, a 2-armed PEG-aldehyde (2-armed PEGAL40k) was used in N-terminal PEGylation which was carried out in 20 mM succinate buffer, pH 6, in the presence of 11.5 μM of sodium cyanoborohydride (NaCNBH$_3$). The concentration of AAT in the reaction mixture was 10 mg·ml$^{-1}$ and the molar ratio of PEGAL to AAT was 2:1. The reaction was carried out overnight with mild agitation at room temperature. Linear or 2-armed PEG-maleimide of 30 kDa or 40 kDa (linear PEGMA30k, PEGMA40k, and 2-armed PEGMA40k) was used for thiol PEGylation on the unique cysteine residue (Cys232). However, Cys232 is cysteinylated.[32] Therefore, to access the thiol group, the purified AAT was first reduced by 1.5 μM tris(2-carboxyethyl) phosphine (TCEP) and then incubated at a concentration of 20 mg·ml$^{-1}$ with PEGMA (molar ratio PEGAL:AAT of 4:1) for 1 hr with mild agitation in 10 mM NaH$_2$PO$_4$, 110 mM NaCl, pH 7.1. Both steps were carried out at room temperature. The PEGylation sites of both reactions are shown in Figure 1.

The mono-PEGylated AAT was purified by anion exchange chromatography using a Mono Q 4.6/100 PE column (GE Healthcare Bio-Sciences AB, Uppsala, Sweden). With 20 mM N(CH$_2$CH$_2$OH)$_3$, 5 mM NaCl, pH 7.5 as the start buffer and 20 mM N(CH$_2$CH$_2$OH)$_3$, 250 mM NaCl, pH 7.5 as the elution buffer. A linear salt gradient elution (between 0 and 100%) was performed. The collected fractions were analyzed by SDS-PAGE followed by silver staining, and the fractions containing the mono-PEGylated AAT were pooled and concentrated using VIVASPIN 15R sample concentrator (10,000 molecular weight cut-off, Sartorius, Stonehouse, Gloucestershire, UK).

## 5.3 | Chemical-induced unfolding

### 5.3.1 | Preparation of samples

The protein concentration was determined by the absorbance at 280 nm where PEG has no signal contribution, using Beer–Lambert Law with the extinction coefficient of 19,940 M$^{-1}$ cm$^{-1}$.[68] Samples containing 0.15 mg·ml$^{-1}$ AAT or PEGylated AAT in DPBS buffer were incubated overnight at 25°C in the presence of various concentrations of GdmCl. The GdmCl concentration of each sample was determined by an R5000 refractometer from ATAGO Co., Ltd. (Tokyo, Japan) using a refractive index measurement.[69] The same samples were used for intrinsic fluorescence and CD measurements. Afterwards, aliquots of the same samples were incubated with 20-fold molar excess of ANS for ANS-bound fluorescence measurements.

### 5.3.2 | Intrinsic fluorescence measurements

The intrinsic fluorescence spectra were recorded at 25°C using a Cary Eclipse fluorescence spectrophotometer equipped with a Peltier cell holder (Varian, Palo Alto, CA), using a 0.4*1 cm pathlength quartz micro-cuvette. The excitation and emission slit widths were both 5 nm and a low scan speed (120 nm/min) was used. The high voltage on the photomultiplicator (PMT) was 870 V. The excitation wavelength was 280 nm, and the emission spectra were recorded between 300 and 460 nm.

The unfolding kinetics study of AAT was carried out as follows: 20 μl of 1 mg·ml$^{-1}$ AAT solution was placed in a 0.4*1 cm pathlength quartz micro-cuvette; 180 μl DPBS or DPBS solution containing 1, 2, 3, 4, and 5 M of GdmCl were added to the cuvette; immediately after mixing the solution, the fluorescence intensity at 350 nm was recorded every 0.1 min for 30 min following excitation at 280 nm; the excitation and emission slit widths were 5 nm, the high voltage on the PMT was 870 V.

### 5.3.3 | Far UV-CD measurements

CD signals were recorded with a J-810 spectropolarimeter equipped with a Peltier cell holder (Jasco International

Co., Ltd., Tokyo, Japan) using a 1-mm pathlength quartz cuvette. The spectra were recorded at 25°C from 190 to 250 nm, with a scan speed of 50 nm·min⁻¹, 1-nm bandwidth and a 2-s integration time. Five spectra were recorded, averaged, and corrected from the contribution of the buffer alone. For GdmCl-induced unfolding, the CD signal at 222 nm was recorded every 5 s for 5 min at 25°C, with a 1-nm bandwidth and a 4-s integration time. The 36 values obtained were averaged and corrected from the contribution of the buffer recorded under the same conditions.

### 5.3.4 | ANS-bound fluorescence measurements

The ANS-bound fluorescence spectra were recorded using the same conditions as above for intrinsic fluorescence except that the excitation wavelength was 350 nm, and the emission spectra were recorded between 400 and 660 nm. The fluorescence intensity at 480 nm (corrected from the contribution of the buffer and GdmCl) was used to monitor the transitions.

### 5.3.5 | Analysis of the data

The chemically-induced unfolding curves were monitored by the fluorescence intensity at 330, 336, and 360 nm, as well as the wavelength of the maximum fluorescence ($\lambda_{max}$), determined from fitting each spectrum with a Weibull five parameters equation model from SigmaPlot 12 (SPSS Inc., Chicago, IL) and the CD signal at 222 nm at 25°C corrected form the contribution of the buffer alone.

The thermodynamic parameters were computed on the assumption of a three-state model for the unfolding reaction (N ⇌ I ⇌ U). The transition curves were analyzed according to the following equation[70]:

$$F = \frac{(F_{N_0} + p[D]) + (F_{I_0}) \times e^{-\alpha} + (F_{U_0} + q[D]) \times e^{-\alpha} e^{-\beta}}{1 + e^{-\alpha} + e^{-\alpha} e^{-\beta}}$$

(1)

where $\alpha = \frac{\Delta G°_{NI(H2O)} - m_{NI}[D]}{RT}$, $\beta = \frac{\Delta G°_{IU(H2O)} - m_{IU}[D]}{RT}$, and where $F$ is the measured parameter (i.e., fluorescence intensity, $\lambda_{max}$ or far UV-CD signal) at a given GdmCl concentration. $F_{N_0}$, $F_{I_0}$, and $F_{U_0}$ represent the values of this parameter for the native ($N$), intermediate ($I$), and unfolded ($U$) states, in the absence of denaturant, respectively. $\Delta G°_{NI}$

(H2O) and $\Delta G°_{IU(H2O)}$ are the difference in free energy between $N$ and $I$, $I$ and $U$ states, respectively. $m_{NI}$ and $m_{IU}$ are the measures of the dependence of the free energy on the denaturant concentration. [$D$] is the denaturant concentration. And $p$, and $q$ are the slopes of the pre-transition, and post-transition baselines, respectively. $R$ is the gas constant, and $T$ is the absolute temperature. $Cm_{NI}$ and $Cm_{IU}$, the denaturant concentration at the midpoint of each transition and are defined as $\Delta°G_{NI}$ (H2O)/$m_{NI}$ and $\Delta°G_{IU (H2O)}$/$m_{IU}$, respectively. GraFit 3.09 (Erithacus Software Ltd., West Sussex, UK) and Sigmaplot 12.0 (SPSS Inc., Chicago, IL) were used to perform the non-linear fit of the data.

## 5.4 | Heat-induced unfolding

### 5.4.1 | Fluorescence measurements

For intrinsic fluorescence measurements, samples containing 0.15 mg·ml⁻¹ AAT or PEGylated AAT were prepared in DPBS buffer at 25°C. A 1-cm pathlength quartz micro-cuvette was used and mineral oil was added on top of the protein solution surface to prevent evaporation. The temperature was linearly increased from 25 to 95°C at 0.5°C·min⁻¹. The excitation wavelength was 280 nm and the fluorescence intensity at 324 nm was recorded every 0.5°C. The excitation and emission slit widths were 5 nm. The high voltage on the PMT was 870 V. The actual temperature inside the sample was recorded using a thermo-couple (PT200 differential thermometer, IMPOT Electronics, Albertslund, Denmark).

### 5.4.2 | Size exclusion chromatography

Samples containing 0.15 mg·ml⁻¹ AAT or PEGylated AAT in DPBS buffer were incubated at 70°C for 1 hour and then cooled down to room temperature. The heating temperature was selected based on the following observations made by Lomas et al.[63]: (a) AAT in sodium citrate only partially losses its activity when incubated at temperature below 70°C for 24 h; (b) AAT tends to remain monomeric until 70°C. Before the SEC analysis, to remove the large aggregates, the samples were filtered through a 0.22-µm cut-off membrane. Samples were analyzed on a Superose 6 Increase 10/300 column (GE Healthcare Bio-Sciences AB, Uppsala, Sweden). The relative content of the monomeric protein was calculated from the peaks integration from the chromatograms.

### 5.4.3 | Dynamic light scattering measurements

Samples containing 1 mg·ml$^{-1}$ AAT or PEGylated AAT in DPBS buffer at 25°C were analyzed in a 1 cm pathlength glass cuvette by Malvern Zetasizer Ultra (Sysmex Belgium NV, Hoeilaart, Belgium) and mineral oil was added on top of the protein solution to prevent evaporation. The temperature was linearly increased from 25 to 95°C at 0.5°C·min$^{-1}$. The hydrodynamic diameters were measured three times every 3°C.

### 5.4.4 | Data analysis for thermal-induced unfolding monitored by intrinsic fluorescence

The thermal unfolding curves monitored by intrinsic fluorescence and ANS-bound fluorescence, were analyzed on the assumption of a two-state transition model using the following equation[71]:

$$F = \frac{(F_N + p[T]) + (F_U + q[T]) \times e^a}{1 + e^a} \quad (2)$$

where $a = \frac{-\Delta H_m \left(1 - \frac{[T]}{T_m}\right)}{RT}$, and where $F$ is the measured variable parameter; $F_N$ and $F_U$ represent the values of this parameter for the native ($N$) and unfolded ($U$) states at 273K. $[T]$ is the measured temperature in Kelvin. $p$ and $q$ are the slopes of the pre-transition and post-transition baselines. $R$ is the gas constant and $T$ is the absolute temperature. $T_m$ is the temperature of mid-transition and $\Delta H_m$ is the enthalpy value at $T_m$. The fluorescence data above 70°C were excluded due to the presence of aggregates in the samples. Since the transitions were not reversible, only the apparent $T_m$ ($T_m^{app}$) was considered for the analysis. GraphPad Prism 8 (GraphPad Software, San Diego, CA) was used to perform the non-linear fit of the data.

### 5.5 | Inhibition of human elastase

The activity of native, refolded or denatured AAT and PEGylated AAT were determined by monitoring their ability to inhibit the activity of human elastase purified from sputum.

The refolded proteins were prepared as follows: AAT or PEGylated AAT were incubated with 6.9 M GdmCl for at least 2 hr to assure the full unfolding of the proteins. Afterwards, microdialysis in DPBS was performed to remove >99.9% of the GdmCl as described previously.[72] The fluorescence spectrum of the refolded samples was recorded to confirm the folded state of the proteins.

The activity of hNE was measured according to Lestienne and Bieth.[73] Briefly, 0.17 μM hNE was incubated with 1.51 mM substrate N-Succinyl-Ala-Ala-Ala-pNitroanilide (Tris-NaCl buffer, pH 7.5) in a 96-well plate for 20 min at 37°C. Afterward, 0.17 μM of refolded or heated AAT or PEGylated AAT samples were added to the mixture and incubated for 40 min. During the incubation, the absorbance at 410 nm of each sample was recorded every 1 min. The changes in absorbance at 410 nm after adding AAT or PEGylated AAT were used to quantify the hNE activity and the relative hNE activity was calculated using the changes of absorbance at 410 nm for hNE alone as control.

### 5.6 | Protein stability to proteolysis by MMP-13

Unconjugated AAT and thiol PEGylated AAT were incubated with matrix metalloproteinase-13 (MMP-13) with a protein:MMP-13 M ratio of 30:1, in 50 mM Tris–HCl, 250 mM NaCl, 5 mM CaCl$_2$, pH 7, at 37°C. MMP-13 was chosen as it has a proteolytic activity on AAT without being inhibited by AAT.[30] After 3, 5, and 27 hr, the remaining activity of AAT or PEG-AAT was evaluated by the elastase inhibition assay as described in Section 5.5 with the protein:hNE molar ratio of 1:1. In parallel, protein samples were incubated in the absence of MMP-13 under the same conditions and was used as positive controls. The remaining hNE activity was used to describe the activity loss of AAT or PEG-AAT.

## ORCID
*Rita Vanbever* https://orcid.org/0000-0002-0784-8771

## REFERENCES

1. Chapman KR, Chorostowska-Wynimko J, Koczulla AR, Ferrarotti I, McElvaney NG. Alpha 1 antitrypsin to treat lung disease in alpha 1 antitrypsin deficiency: Recent developments and clinical implications. Int J Chron Obstruct Pulmon Dis. 2018;13:419–432.

2. Korkmaz B, Attucci S, Jourdan M-L, Juliano L, Gauthier F. Inhibition of neutrophil elastase by alpha1-protease inhibitor at the surface of human polymorphonuclear neutrophils. J Immunol. 2005;175(5):3329–3338.

3. Duranton J, Bieth JG. Inhibition of proteinase 3 by alpha1-antitrypsin in vitro predicts very fast inhibition in vivo. Am J Respir Cell Mol Biol. 2003;29(1):57–61.

4. Padrines M, Schneider-Pozzer M, Bieth JG. Inhibition of neutrophil elastase by Alpha-1-proteinase inhibitor oxidized by activated neutrophils. Am Rev Respir Dis. 1989;139(3):783–790.

5. Tonelli AR, Brantly ML. Augmentation therapy in alpha-1 antitrypsin deficiency: Advances and controversies. Ther Adv Respir Dis. 2010;4(5):289–312.

6. Stolk J, Tov N, Chapman KR, et al. Efficacy and safety of inhaled α1-antitrypsin in patients with severe α1-antitrypsin deficiency and frequent exacerbations of COPD. Eur Respir J. 2019;54(5):1900673.

7. Pasut G, Veronese FM. State of the art in PEGylation: The great versatility achieved after forty years of research. J Control Release. 2012;161(2):461–472.

8. Turecek PL, Bossard MJ, Schoetens F, Ivens IA. PEGylation of biopharmaceuticals: A review of chemistry and nonclinical safety information of approved drugs. J Pharm Sci. 2016;105(2): 460–475.

9. Rondon A, Mahri S, Morales-Yanez F, Dumoulin M, Vanbever R. Protein engineering strategies for improved pharmacokinetics. Adv Funct Mater. 2021;31(44):2101633.

10. Veronese FM, Pasut G. PEGylation, successful approach to drug delivery. Drug Discov Today. 2005;10(21):1451–1458.

11. Wu L, Ho SV, Wang W, et al. N-terminal mono-PEGylation of growth hormone antagonist: Correlation of PEG size and pharmacodynamic behavior. Int J Pharm. 2013;453(2):533–540.

12. Veronese FM, Mero A. The impact of PEGylation on biological therapies. BioDrugs. 2008;22(5):315–329.

13. Lawrence PB, Price JL. How PEGylation influences protein conformational stability. Curr Opin Chem Biol. 2016;34:88–94.

14. Frokjaer S, Otzen DE. Protein drug stability: A formulation challenge. Nat Rev Drug Discov. 2005;4(4):298–306.

15. Jain A, Ashbaugh HS. Helix stabilization of poly(ethylene glycol)-peptide conjugates. Biomacromolecules. 2011;12(7):2729–2734.

16. Price JL, Powers ET, Kelly JW. N-PEGylation of a reverse turn is stabilizing in multiple sequence contexts, unlike N-GlcNAcylation. ACS Chem Biol. 2011;6(11):1188–1192.

17. Rodríguez-Martínez JA, Solá RJ, Castillo B, et al. Stabilization of alpha-chymotrypsin upon PEGylation correlates with reduced structural dynamics. Biotechnol Bioeng. 2008;101(6): 1142–1149.

18. García-Arellano H, Valderrama B, Saab-Rincón G, Vazquez-Duhalt R. High temperature biocatalysis by chemically modified cytochrome c. Bioconjug Chem. 2002;13(6):1336–1344.

19. Plesner B, Fee CJ, Westh P, Nielsen AD. Effects of PEG size on structure, function and stability of PEGylated BSA. Eur J Pharm Biopharm. 2011;79(2):399–405.

20. Rodríguez-Martínez JA, Rivera-Rivera I, Griebenow K. Prevention of benzyl alcohol-induced aggregation of chymotrypsinogen by PEGylation. J Pharm Pharmacol. 2011;63(6):800–805.

21. Shu JY, Tan C, DeGrado WF, Xu T. New design of helix bundle peptide-polymer conjugates. Biomacromolecules. 2008;9(8): 2111–2117.

22. Lawrence PB, Gavrilov Y, Matthews SS, et al. Criteria for selecting PEGylation sites on proteins for higher thermodynamic and proteolytic stability. J Am Chem Soc. 2014;136(50): 17547–17560.

23. Knaupp AS, Bottomley SP. Structural change in β-sheet A of Z α(1)-antitrypsin is responsible for accelerated polymerization and disease. J Mol Biol. 2011;413(4):888–898.

24. Guex N, Peitsch MC, Schwede T. Automated comparative protein structure modeling with SWISS-MODEL and Swiss-PdbViewer: A historical perspective. Electrophoresis. 2009;30-(Suppl 1):S162–S173.

25. Tew DJ, Bottomley SP. Probing the equilibrium denaturation of the serpin alpha(1)-antitrypsin with single tryptophan mutants; evidence for structure in the urea unfolded state. J Mol Biol. 2001;313(5):1161–1169.

26. Patschull AOM, Gooptu B, Ashford P, Daviter T, Nobeli I. In silico assessment of potential druggable pockets on the surface of α1-antitrypsin conformers. PLoS ONE. 2012;7(5):e36612.

27. Dasi Sangachini E, Hasannia S, Taghdir M, Pirooznia N, Khalili GK. Construction of an engineered alpha 1-antitrypsin with inhibitory activity based on theoretical studies. Electron J Biotechnol. 2012;15(2):8.

28. Gasymov OK, Glasgow BJ. ANS fluorescence: Potential to augment the identification of the external binding sites of proteins. Biochim Biophys Acta. 2007;1774(3):403–411.

29. Janciauskiene S, Wrenger S, Immenschuh S, et al. The multifaceted effects of Alpha1-antitrypsin on neutrophil functions. Front Pharmacol. 2018;9:341.

30. Elkington PTG, Friedland JS. Matrix metalloproteinases in destructive pulmonary pathology. Thorax. 2006;61(3):259–266.

31. Pandey KC, De S, Mishra PK. Role of proteases in chronic obstructive pulmonary disease. Front Pharmacol. 2017;8:512.

32. Liu X, Vanvarenberg K, Guy Wilfried Kouassi K, Mahri S, Vanbever R. Production and characterization of mono-PEGylated alpha-1 antitrypsin for augmentation therapy. Int J Pharm. 2022;612:121355.

33. Cantin AM, Woods DE, Cloutier D, Dufour EK, Leduc R. Polyethylene glycol conjugation at Cys232 prolongs the half-life of alpha1 proteinase inhibitor. Am J Respir Cell Mol Biol. 2002; 27(6):659–665.

34. Chiu K, Agoubi LL, Lee I, Limpar MT, Lowe JW, Goh SL. Effects of polymer molecular weight on the size, activity, and stability of PEG-functionalized trypsin. Biomacromolecules. 2010;11(12):3688–3692.

35. Guichard M-J, Patil HP, Koussoroplis SJ, Wattiez R, Leal T, Vanbever R. Production and characterization of a PEGylated derivative of recombinant human deoxyribonuclease I for cystic fibrosis therapy. Int J Pharm. 2017;524(1–2):159–167.

36. Plesner B, Westh P, Nielsen AD. Biophysical characterisation of GlycoPEGylated recombinant human factor VIIa. Int J Pharm. 2011;406(1–2):62–68.

37. Kolarich D, Turecek PL, Weber A, et al. Biochemical, molecular characterization, and glycoproteomic analyses of alpha(1)-proteinase inhibitor products used for replacement therapy. Transfusion. 2006;46(11):1959–1977.

38. Luo S, Lu X, Liu C, Zhong J, Zhou L, Chen T. Site specific PEGylation of β-lactoglobulin at glutamine residues and its influence on conformation and antigenicity. Food Res Int. 2019;123:623–630.

39. Mero A, Grigoletto A, Maso K, Yoshioka H, Rosato A, Pasut G. Site-selective enzymatic chemistry for polymer conjugation to protein lysine residues: PEGylation of G-CSF at lysine-41. Polym Chem. 2016;7(42):6545–6553.

40. Wang J, Hu T, Liu Y, Zhang G, Ma G, Su Z. Kinetic and stoichiometric analysis of the modification process for N-terminal PEGylation of staphylokinase. Anal Biochem. 2011;412(1):114–116.

41. Suo X, Lu X, Hu T, Ma G, Su Z. A solid-phase adsorption method for PEGylation of human serum albumin and staphylokinase: Preparation, purification and biochemical characterization. Biotechnol Lett. 2009;31(8):1191–1196.

42. Zhu W, Li L, Deng M, et al. Oxidation-resistant and thermostable forms of alpha-1 antitrypsin from Escherichia coli inclusion bodies. FEBS Open Bio. 2018;8(10):1711–1721.

43. Tsutsui Y, Wintrode PL. Cooperative unfolding of a metastable serpin to a molten globule suggests a link between functional and folding energy landscapes. J Mol Biol. 2007;371(1):245–255.

44. Krishnan B, Gierasch LM. Dynamic local unfolding in the serpin α-1 antitrypsin provides a mechanism for loop insertion and polymerization. Nat Struct Mol Biol. 2011;18(2):222–226.

45. Knaupp AS, Levina V, Robertson AL, Pearce MC, Bottomley SP. Kinetic instability of the serpin Z alpha1-antitrypsin promotes aggregation. J Mol Biol. 2010;396(2):375–383.

46. Dobó J, Gettins PGW. alpha1-proteinase inhibitor forms initial non-covalent and final covalent complexes with elastase analogously to other serpin-proteinase pairs, suggesting a common mechanism of inhibition. J Biol Chem. 2004;279(10):9264–9269.

47. Tran ST, Shrake A. The folding of alpha-1-proteinase inhibitor: Kinetic vs equilibrium control. Arch Biochem Biophys. 2001;385(2):322–331.

48. Sorret LL, Monticello CR, DeWinter MA, Schwartz DK, Randolph TW. Steric repulsion forces contributed by PEGylation of interleukin-1 receptor antagonist reduce gelation and aggregation at the silicone oil–water interface. J Pharm Sci. 2019;108(1):162–172.

49. Elliott PR, Abrahams JP, Lomas DA. Wild-type alpha 1-antitrypsin is in the canonical inhibitory conformation. J Mol Biol. 1998;275(3):419–425.

50. Bottomley SP. The folding pathway of alpha1-antitrypsin: Avoiding the unavoidable. Proc Am Thorac Soc. 2010;7(6):404–407.

51. Tsutsui Y, Dela Cruz R, Wintrode PL. Folding mechanism of the metastable serpin α1-antitrypsin. Proc Natl Acad Sci U S A. 2012;109(12):4467–4472.

52. Kang U-B, Baek J-H, Ryu S-H, Kim J, Yu M-H, Lee C. Kinetic mechanism of protease inhibition by alpha1-antitrypsin. Biochem Biophys Res Commun. 2004;323(2):409–415.

53. Ali MF, Kaushik A, Kapil C, Gupta D, Jairajpuri MA. A hydrophobic patch surrounding Trp154 in human neuroserpin controls the helix F dynamics with implications in inhibition and aggregation. Sci Rep. 2017;7:42987.

54. Mallya M, Phillips RL, Saldanha SA, et al. Small molecules block the polymerization of Z alpha1-antitrypsin and increase the clearance of intracellular aggregates. J Med Chem. 2007;50(22):5357–5363.

55. Chang Y-P, Mahadeva R, Chang W-SW, Lin S-C, Chu Y-H. Small-molecule peptides inhibit Z alpha1-antitrypsin polymerization. J Cell Mol Med. 2009;13(8B):2304–2316.

56. Kwon K-S, Yu M-H. Effect of glycosylation on the stability of α1-antitrypsin toward urea denaturation and thermal deactivation. Biochim Biophys Acta. 1997;1335(3):265–272.

57. Lomas DA, Evans DL, Stone SR, Chang WS, Carrell RW. Effect of the Z mutation on the physical and inhibitory properties of alpha 1-antitrypsin. Biochemistry. 1993;32(2):500–508.

58. Haq I, Irving JA, Saleh AD, et al. Deficiency mutations of alpha-1 antitrypsin effects on folding, function, and polymerization. Am J Respir Cell Mol Biol. 2016;54(1):71–80.

59. Roque C, Sheung A, Rahman N, Ausar SF. Effect of polyethylene glycol conjugation on conformational and colloidal stability of a monoclonal antibody antigen-binding fragment (fab'). Mol Pharm. 2015;12(2):562–575.

60. Rajan RS, Li T, Aras M, et al. Modulation of protein aggregation by polyethylene glycol conjugation: GCSF as a case study. Protein Sci. 2006;15(5):1063–1075.

61. Veronese FM, Mero A, Caboi F, Sergi M, Marongiu C, Pasut G. Site-specific pegylation of G-CSF by reversible denaturation. Bioconjug Chem. 2007;18(6):1824–1830.

62. Persson C, Subramaniyam D, Stevens T, Janciauskiene S. Do native and polymeric alpha1-antitrypsin activate human neutrophils in vitro? Chest. 2006;129(6):1683–1692.

63. Lomas DA, Elliott PR, Chang WS, Wardell MR, Carrell RW. Preparation and characterization of latent alpha 1-antitrypsin. J Biol Chem. 1995;270(10):5282–5288.

64. Janciauskiene S, Dominaitiene R, Sternby NH, Piitulainen E, Eriksson S. Detection of circulating and endothelial cell polymers of Z and wild type alpha 1-antitrypsin by a monoclonal antibody. J Biol Chem. 2002;277(29):26540–26546.

65. Zhang C, Desai R, Perez-Luna V, Karuri N. PEGylation of lysine residues improves the proteolytic stability of fibronectin while retaining biological activity. Biotechnol J. 2014;9(8):1033–1043.

66. Zhang C, Hekmatfar S, Ramanathan A, Karuri NW. PEGylated human plasma fibronectin is proteolytically stable, supports cell adhesion, cell migration, focal adhesion assembly, and fibronectin fibrillogenesis. Biotechnol Prog. 2013;29(2):493–504.

67. Danial M, van Dulmen THH, Aleksandrowicz J, Pötgens AJG, Klok H-A. Site-specific PEGylation of HR2 peptides: Effects of PEG conjugation position and chain length on HIV-1 membrane fusion inhibition and proteolytic degradation. Bioconjug Chem. 2012;23(8):1648–1660.

68. Chen Y, Snyder MR, Zhu Y, et al. Simultaneous phenotyping and quantification of α-1-antitrypsin by liquid chromatography–tandem mass spectrometry. Clin Chem. 2011;57(8):1161–1168.

69. Pace CN. Determination and analysis of urea and guanidine hydrochloride denaturation curves. Methods Enzymol. 1986; 131:266–280.

70. Vandenameele J, Lejeune A, Di Paolo A, et al. Folding of class a beta-lactamases is rate-limited by peptide bond isomerization and occurs via parallel pathways. Biochemistry. 2010;49(19): 4264–4275.

71. El Hajjaji H, Dumoulin M, Matagne A, et al. The zinc center influences the redox and thermodynamic properties of Escherichia coli thioredoxin 2. J Mol Biol. 2009;386(1):60–71.

72. Overall CM. A microtechnique for dialysis of small volume solutions with quantitative recoveries. Anal Biochem. 1987; 165(1):208–214.

73. Lestienne P, Bieth JG. The inhibition of human leukocyte elastase by basic pancreatic trypsin inhibitor. Arch Biochem Biophys. 1978;190(1):358–360.

## SUPPORTING INFORMATION

Additional supporting information can be found online in the Supporting Information section at the end of this article.